Journal of Solid State Chemistry 182 (2009) 2362–2367

Contents lists available at ScienceDirect

Journal of Solid State Chemistry

journal homepage: www.elsevier.com/locate/jssc

Liquid phase deposition synthesis of hexagonal molybdenum trioxide thin films

Shigehito Deki, Alexis Bienvenu Béléké, Yuki Kotani, Minoru Mizuhata *

Department of Chemical Science and Engineering, Graduate School of Engineering, Kobe University, 1-1 Rokko, Nada, Kobe 657-8501, Japan

ARTICLE INFO

Article history:
Received 17 March 2009
Received in revised form
18 June 2009
Accepted 20 June 2009
Available online 27 June 2009

Keywords:
Hexagonal molybdenum trioxide
Hydrates
Thin film
Liquid phase deposition

ABSTRACT

Hexagonal molybdenum trioxide thin films with good crystallinity and high purity have been fabricated by the liquid phase deposition (LPD) technique using molybdic acid (H_2MoO_4) dissolved in 2.82% hydrofluoric acid (HF) and H_3BO_3 as precursors. The crystal was found to belong to a hexagonal hydrate system $MoO_3.nH_2O$ (n∼0.56). The unit cell lattice parameters are $a = 10.651$ Å, $c = 3.725$ Å and $V = 365.997$ Å^3. Scanning electron microscope (SEM) images of the as-deposited samples showed well-shaped hexagonal rods nuclei that grew and where the amount increased with increase in reaction time. X-ray photon electron spectroscopy (XPS) spectra showed a Gaussian shape of the doublet of Mo 3d core level, indicating the presence of Mo^{6+} oxidation state in the deposited films. The deposited films exhibited an electrochromic behavior by lithium intercalation and deintercalation, which resulted in coloration and bleaching of the film. Upon dehydration at about 450 °C, the hexagonal $MoO_3.nH_2O$ was transformed into the thermodynamically stable orthorhombic phase.

1. Introduction

Molybdenum trioxide is one of the transition metal oxide materials widely investigated due to its distinctive properties that enable it to function as an active component in supported catalysts [1], displays [2], imaging and gas-sensing devices [3], smart windows [4] and electrodes of rechargeable ion batteries [5]. Its crystalline structure is known to exist under three polymorphs: one thermodynamically stable phase α-MoO_3 [6] and two metastable phases, β-MoO_3 analogue of WO_3 [7] and hexagonal h-MoO_3 [8]. The MoO_6 octahedron is the basic building unit in all these MoO_3 structures. In orthorhombic α-MoO_3, the MoO_6 octahedra share edges and corners, resulting in a zigzag chain and a unique layer structure [6]. The monoclinic β-MoO_3 has a ReO_3-related structure in which the MoO_6 octahedra share corners to form a distorted cube [9]. The hexagonal h-MoO_3 is also constructed in the same zigzag chains of MoO_6 octahedra but they connect through the *cis*-position between chains [10,11].

Several research efforts have been focused on synthesis and characterization of MoO_3 materials in the form of thin films, nanorods, nanobelts, nanocrystal, etc. A number of techniques that include pulsed laser ablation [12,13], sputtering [14], thermal evaporation [15], chemical vapor deposition (CVD) [16], electro-deposition [17], sol–gel [18], spin coating [19], hydrothermal treatment [20], and hot-filament metal oxide deposition [21] have been proposed for the fabrication of MoO_3 films. It is well known that the microstructure, composition, properties and device applications of thin films depend on the method used to grow the films and processing conditions. In this context, controlling the film growth of metal oxides under mild synthetic conditions is appealing in order to scale-up material synthesis and a precise control of the structure. Therefore, any attempt to fabricate thin films with a novel approach is a matter of great importance.

We have developed a novel technique of preparation of metal oxides and/or thin films with large surface area and complex morphology including nanomaterials [22], highly nano-ordered materials [23], and functionally graded materials [24], called the liquid phase deposition (LPD) method. The basic concepts of the LPD method and its distinction with other solution routes have been described elsewhere [22–29]. The main reactions can be expressed as follows:

$$MF_x^{(x-2n)-} + nH_2O = MO_n + xF^- + 2nH^+$$

$$H_3BO_3 + 4HF = BF^{4-} + H_3O^+ + 2H_2O$$

This method offers the possibility to control the size and the film growth as well as some other advantages such as purity, crystallinity and pH-free control. In this work, we have applied the LPD method to synthesize MoO_3 thin films in order to evaluate its viability, and compare with those obtained by other techniques. A number of characterization techniques have been used to investigate the crystalline structure, morphology and chemical

* Corresponding author. Fax: +81788036186.
E-mail address: mizuhata@kobe-u.ac.jp (M. Mizuhata).

0022-4596/$ - see front matter © 2009 Elsevier Inc. All rights reserved.
doi:10.1016/j.jssc.2009.06.033

states of elements contained in the thin films. In addition, preliminary electrochromic properties were studied by cyclic voltammetry.

2. Experimental section

2.1. Sample preparation

Molybdic acid (H_2MoO_4; Nacalai Tesque Inc.) was dissolved in 2.82% hydrofluoric acid (HF; Stella Chemifa Inc.) aqueous solution at a concentration of 0.5 mol dm^{-3}, and it was used as the parent solution. Boric acid (H_3BO_3; Nacalai Tesque Inc.) was dissolved in distilled water at a concentration of 0.5 mol dm^{-3} and used as the reagent, which acts as F^- scavenger. These two solutions were then mixed together and served as the reaction solution. Final concentrations of H_2MoO_4 and H_3BO_3 in the reaction solution were 0.2 and 0.3 mol dm^{-3}, respectively.

Sapphire plate (1–102), α-Al_2O_3 plate and ITO glass were used as substrates. After degreasing and washing ultrasonically, the substrates were immersed in the reaction solution and suspended therein vertically for various periods of time ranging from 1 to 36 h. The reaction temperature was kept at 40 °C. After each appropriate reaction time, the samples were taken out from the solution, washed with distilled water, and dried at room temperature. Some of the samples were heat treated at 500 and 600 °C for 1 h in a muffle furnace under air flow.

2.2. Characterization of the deposited films

The obtained thin films were characterized by field emission scanning electron microscopy (FE-SEM; JEOL JSM-6335F), an X-ray diffractometer (XRD; RINT-TTR/S2 Rigaku Co. Ltd.) and an X-ray photoelectron spectrometer (XPS; JEOL JPS-9010MC) according to the same procedures as described in our previous work [28]. The amount of Mo contained in deposited film was measured by inductively coupled plasma atomic emission spectrometry (ICP-AES; HORIBA Ltd., ULTIMA 2000). The deposited films on the substrate were dissolved in diluted ammonia solution.

TEM observations of the deposited films were performed using JEOL2010 high-resolution transmission electron microscopy (HRTEM). For the cross-sectional observations, the deposited film was peeled off from the glass substrate in the form of powder, which was dipped into an epoxy matrix followed by curing at 30 °C for 72 h. Thin cross-sectional layers were obtained using Leica Ultracut UCT ultramicrotome.

Thermo-gravimetric (TG) analysis and differential thermal analysis (DTA) measurements were committed from ambient temperature to 500 °C at a heating rate of 10 °C min^{-1} in ambient atmosphere using Thermo Plus 8120 (Rigaku Co. Ltd.).

2.3. Electrical properties

Cyclic voltammetry was performed in a classical three-electrode electrochemical cell using VoltaLab (Radio Analytical S.A. PGZ 402 674R076 N005). A MoO_3 film (1 cm^2) onto indium tin oxide (ITO)-coated glass substrate was adopted as the working electrode whereas a Pt plate (1 cm^2) was used as the counter electrode and Ag/AgCl/KCl served as the reference electrode. The electrodes were immersed in 1 M $LiClO_4$-PC electrolyte solution purged with nitrogen. Measurements were conducted in the range from −0.6 to +1.5 V at a sweep rate of 1 mV/s.

3. Results and discussion

3.1. Film formation

Fig. 1 shows SEM images of the as-deposited films on sapphire at various reaction times ranging from 1 to 36 h. It can be seen that after 1 h (Fig. 1a), hexagonal prismatic crystal nuclei were deposited on sapphire. As the reaction progressed, the number of nuclei increased and the nuclei grew bigger in parallel. After 36 h (Fig. 1i), the substrates were completely covered with a white film

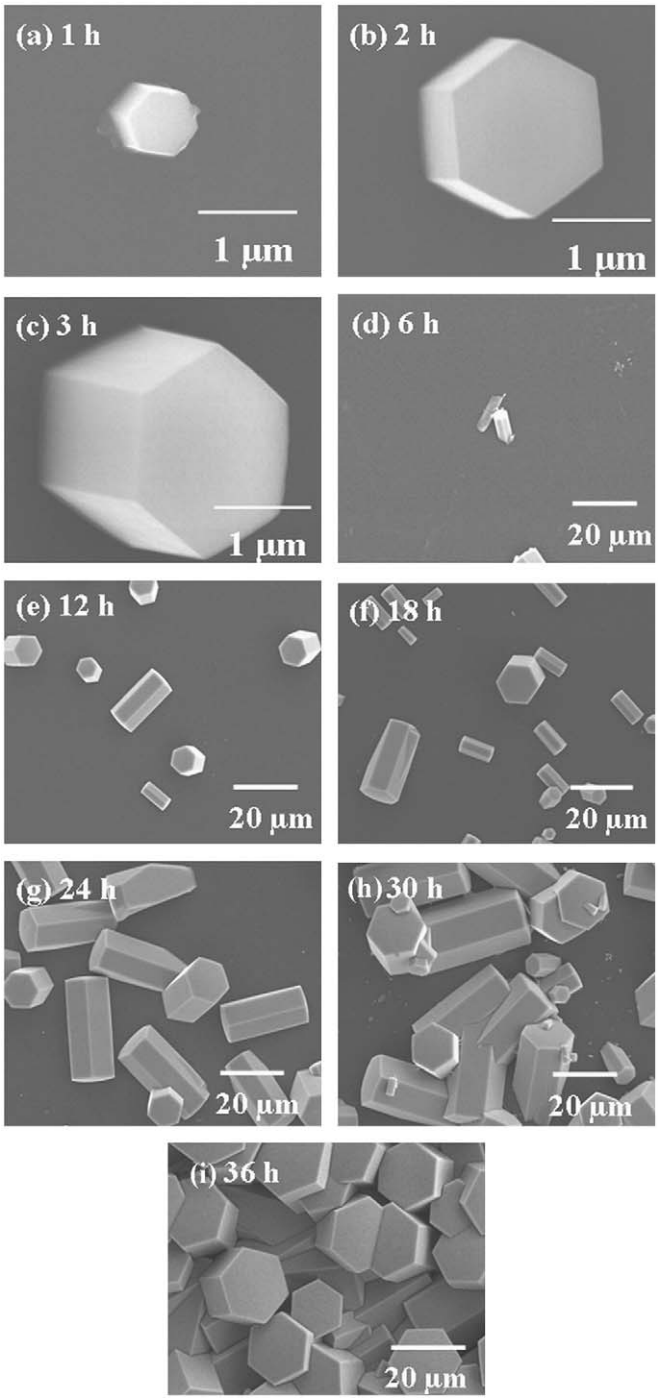

Fig. 1. SEM images of as-deposited MoO_3 films on sapphire at various reaction times. [Mo^{6+}]: 0.2 mol dm^{-3}, [H_3BO_3]: 0.3 mol dm^{-3}.

made of uniform and regular hexagonal rods with a diameter of ca. 16 μm and a length of ca. 30 μm. These images clearly suggest that film growth can be controlled by reaction time. This assumption is corroborated by the evolution of the amount of Mo in the deposited films as a function of reaction time, as shown in Fig. 2. It appears that after a short constant period time called "induction period" in which free F^- released from the metal fluoro-complex in Eq. (1) is consumed according to Eq. (2), the amount of Mo increased exponentially with reaction time.

The diameter and length of the thin film rods obtained in this work after 36 h reaction time are 1.6 and 3 times bigger than the average diameter and length, respectively, of those prepared by a simple precipitation method [30], and are far more bigger than the nanorods fabricated via the probe sonication route [31]. The length of 30 μm is found to be the same as that of the *h*-MoO_3 nanocrystals obtained by Atuchin et al. [32] and recently by Ramana et al. [33] while the cross-sectional size (or diameter) is extremely large, leading to an estimated aspect ratio (length/diameter) of 1.875, which is 32 times lower than that by these authors. Despite the high aspect ratio, attempt to control the size and shape of hexagonal rods by monitoring either the temperature or reaction time was unsuccessful, which is a limitation of the precipitation method, compared to the LPD method which guaranties the shape and size control by tuning the reaction time.

The difference in the form of the final product (nanocrystals by precipitation method versus thin films by LPD method) and in the aspect ratio of the rods confirms that the properties of MoO_3 materials vary and depend on the growth conditions. It is important to specify that the deposition rate in the LPD process is influenced by the degree of supersaturation, which is related to the temperature of the solution and the quantity of added boric acid. Since precursor species are not replenished during the reaction, the deposition rate will decrease once the reactants are used up.

3.2. Structural analysis

Typical XRD patterns of the as-deposited films (a) before and after annealing at (b) 500 °C and (c) 600 °C are shown in Fig. 3. The diffraction data for the as-deposited films are summarized in Table 1. The features in Fig. 3a could be indexed to a hexagonal $MoO_3.nH_2O$, and are consistent with those reported in the literature. [8,10,11,33,34] The unit cell lattice parameters are $a = 10.651$ Å, $c = 3.725$ Å and $V = 365.997$ Å^3. Diffraction patterns in Fig. 3b and c clearly show characteristics of stable orthorhombic α-MoO_3, indicating that the phase transformation was completely achieved above 450 °C. The values of the d-spacing of the obtained orthorhombic MoO_3 phase are in good agreement with JCPDS card no 05–508. The comparison of XRD patterns did not show any significant difference in terms of the intensities of the diffraction peaks between the as-deposited films and the heat-treated ones. This observation suggests that the as-deposited hexagonal MoO_3 hydrate phase is well-crystallized without heat treatment.

The corresponding SEM images showing changes at the surface morphologies of the films deposited on sapphire (a) before and after annealing at (b) 500 °C and (c) 600 °C are illustrated in Fig. 4.

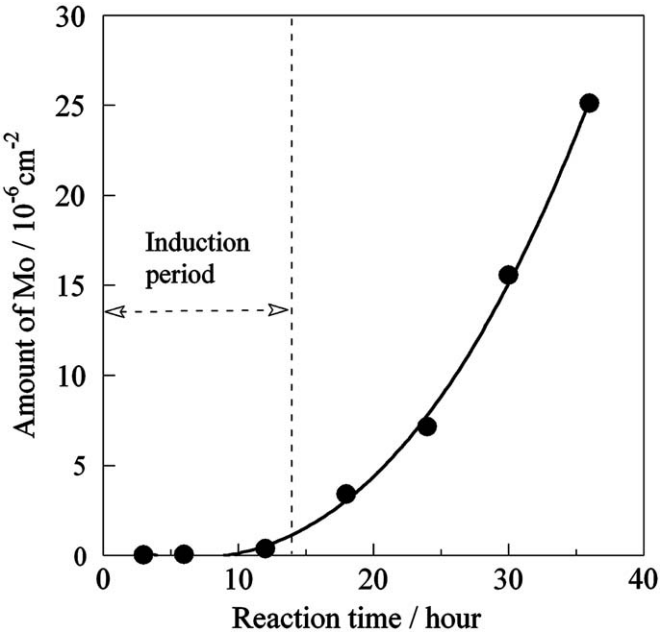

Fig. 2. Amount of Mo in the deposited films on sapphire substrate as a function of reaction time. [Mo^{6+}]: 0.2 mol dm^{-3}, [H_3BO_3]: 0.3 mol dm^{-3}.

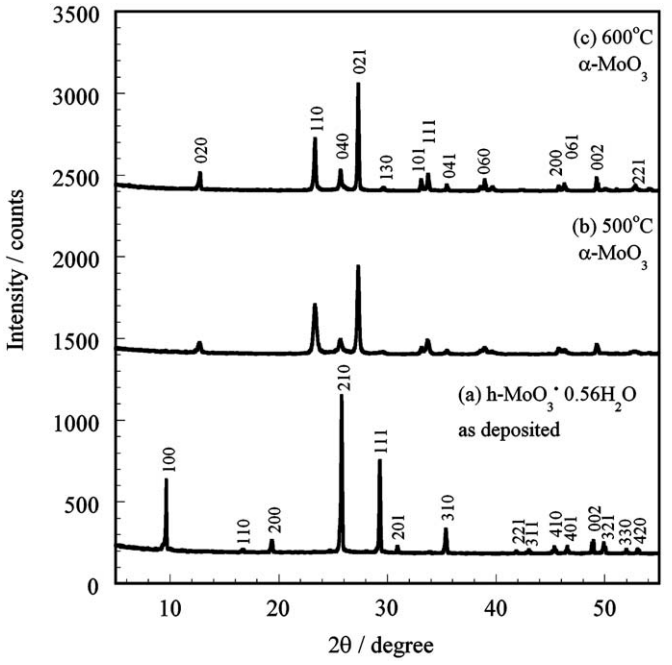

Fig. 3. XRD patterns of MoO_3 films deposited on sapphire substrate after 36 h: (a) as-deposited and after annealing at (b) 500 °C; (c) 600 °C. [Mo^{6+}]: 0.2 mol dm^{-3}, [H_3BO_3]: 0.3 mol dm^{-3}.

Table 1
XRD data of the as-deposited $MoO_3.0.56H_2O$ on sapphire substrate after 36 h.

h	*k*	*l*	$2\theta_{obs}$ (deg.)	d_{obs} (Å)	d_{calc} (Å)
1	0	0	9.577	9.224	9.119
1	1	0	16.795	5.272	5.265
2	0	0	19.436	4.561	4.559
2	1	0	25.774	3.452	3.446
3	0	0	29.295	3.045	3.039
2	0	1	30.88	2.892	2.881
2	2	0	33.873	2.643	2.632
3	1	0	35.457	2.528	2.529
2	2	1	41.795	2.158	2.148
3	1	1	43.204	2.091	2.092
4	1	0	45.492	1.991	1.989
4	0	1	46.549	1.948	1.943
0	0	2	48.838	1.862	1.86
3	2	1	49.894	1.825	1.824
3	3	0	52.007	1.756	1.755

It can be easily seen from this figure that the regular prismatic hexagonal shape of the as-deposited MoO_3 films was affected by heat treatment. At 500 °C (4b), the nuclei cracked after dehydration although they maintained the hexagonal shape. Finally, the hexagonal prisms were completely transformed into plate-like crystals at 600 °C (4c). The difference between the sample morphology at 500 and 600 °C is obviously due to the heating exposure time. There is no change in the structure of the sample as shown by XRD data where both patterns are indexed to the orthorhombic phase. Thus, the morphology at 500 °C is an intermediate phase preceding the final orthorhombic structure shown at 600 °C. In other terms, a longer heating exposure time at 500 °C would result in the same feature as in Fig. 6c. This assumption is supported by both TG and DTA data (see supporting information). An exothermic peak observed (in DTA curve) at 430 °C characterizes the structural transformation from hexagonal to stable orthorhombic MoO_3 phase (α-MoO_3). Finally, on heating above 430 °C, anhydrous orthorhombic MoO_3 is obtained. (This undermines the fact that the morphology at 500 °C is an intermediate state of the thermodynamically stable orthorhombic phase.)

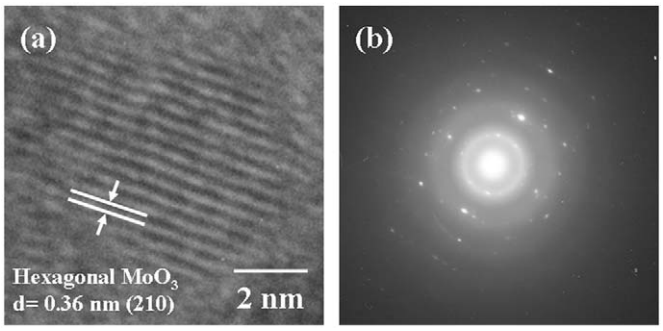

Fig. 4. Surface morphologies of the deposited films on sapphire substrate after 36 h: (a) as-deposited and after annealing at (b) 500 °C; (c) 600 °C. [Mo^{6+}]: 0.2 mol dm^{-3}, [H_3BO_3]: 0.3 mol dm^{-3}.

Thermo-gravimetric analysis (not shown) revealed a total weight loss of 6.6% corresponding to 0.56 mol of water per MoO_3, which confers the chemical formulae of $MoO_3.0.56H_2O$. However, the amount of water is indefinite and could slightly vary with the conditions of preparation. This amount of water lies between the values contained in the hexagonal molybdenum

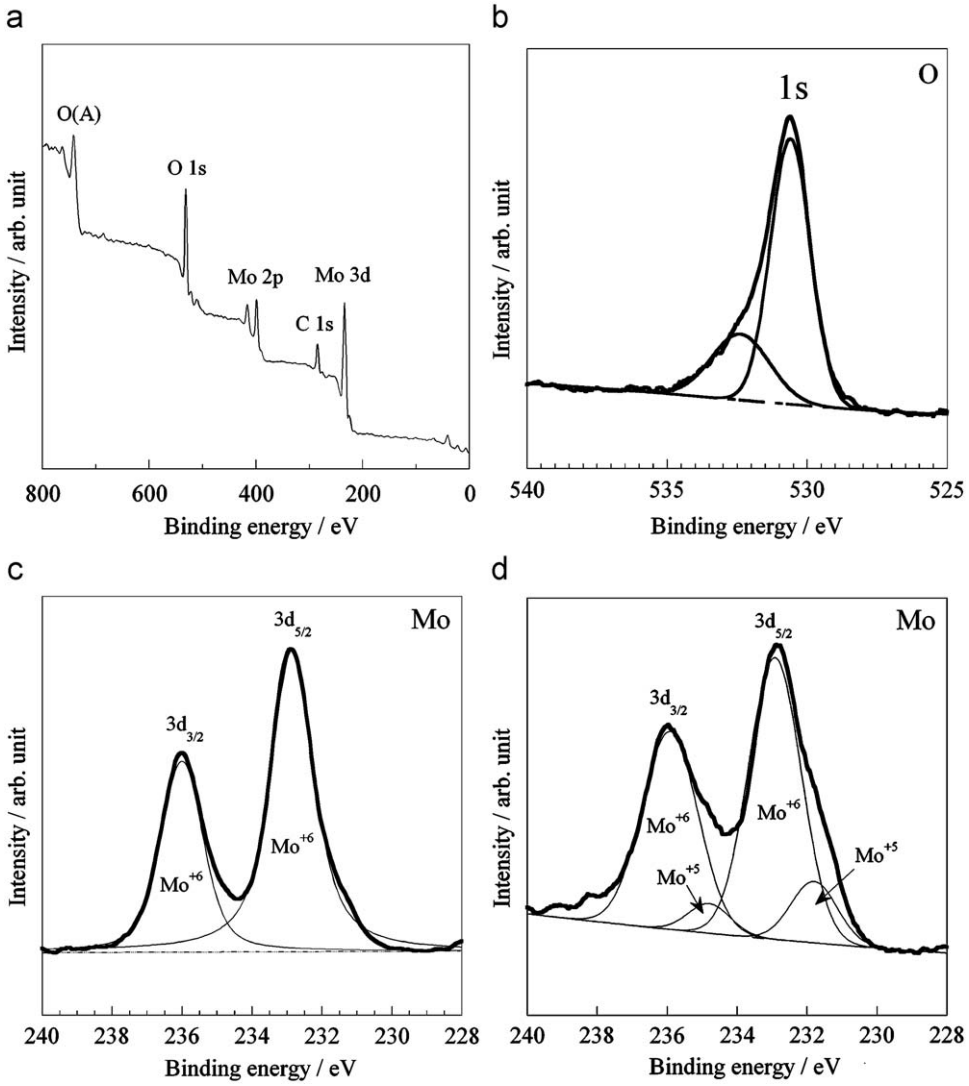

Fig. 5. (a) High-resolution TEM image and (b) the corresponding electron diffraction of the as-deposited MoO_3 on sapphire substrate after 36 h. [Mo^{6+}]: 0.2 mol dm^{-3}, [H_3BO_3]: 0.3 mol dm^{-3}.

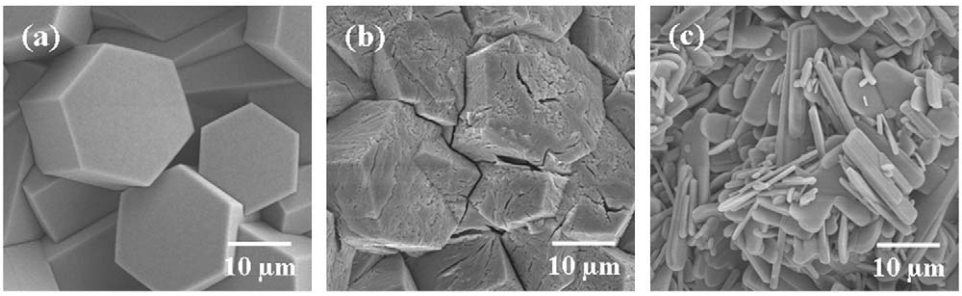

Fig. 6. XPS spectra of MoO_3 film deposited on ITO glass substrate after 36 h. (a) Mo 3*d* core level before, (b) Mo 3*d* core level after insertion of lithium. [Mo^{6+}]: 0.2 mol dm^{-3}, [H_3BO_3]: 0.3 mol dm^{-3}.

trioxide hydrates prepared by Sotani [11] and Guo [10], respectively.

For further investigation on the crystalline structure of the as-deposited film, TEM observations and selected area electron diffraction (SAED) analysis are shown in Fig. 5. The lattice spacing estimated to ca. 0.37 nm (Fig. 5a) is assigned to the *h*-MoO_3 index (2 1 0). Furthermore, the appearance of the well-defined reflection spots on the corresponding electron diffraction pattern (Fig. 5b) confirms that the as-deposited films are oriented in some degree.

It is noteworthy to mention that the LPD thin films maintained strong adherence to the substrate even after heat treatment. This aspect was demonstrated in our previous work on the growth of iron oxyhydroxide (β-FeOOH) thin film deposited on Au substrate where high-resolution transmission electron microscopy image near the film/substrate interface indicated that the films showed strong adherence to the substrate with epitaxial growing of oxide film even at the solid/liquid interface [35].

3.3. XPS analysis

In order to identify the material quality, compositional analysis of the as-deposited films was carried out by XPS. Survey scan information of this spectroscopic analysis is useful, particularly in terms of identifying the elements present at the film surface. Fig. 6a shows the XPS survey spectrum acquired from the surface of the as-deposited films, which displays only peaks corresponding to Mo3d, O 1*s* and C 1*s*. These peak positions are in good agreement with those found by other researchers. [17,36–38] The absence of any extra element in this qualitative survey scan analysis infers the compositional purity of the LPD-based $MoO_3.nH_2O$ films.

The deconvolution using Gaussian–Lorentzian curve-fitting function of the O 1*s* peak in Fig. 6b shows two components: an intense peak at a binding energy of 530.6 eV assigned to crystal bulk oxygen in MoO_3 [36,38] and a broadened one at 532.4 eV related to oxygen in water molecules bound in the film structure or adsorbed species [15]. In Fig. 6(c and d), the XPS core level of Mo 3*d* spectra for the deposited MoO_3 film before and after lithium insertion are shown, respectively. The doublet pattern observed for MoO_3 (Fig. 6c) is due to the spin orbit splitting of Mo 3d levels giving rise to Mo $3d_{3/2}$ and Mo $3d_{5/2}$ levels with an energy separation of 3.15 eV. The deconvolution exhibits two components with binding energies at 235.8 and 232.7 eV, respectively, identified as the energies of the 3*d* doublet of Mo^{6+} ions in MoO_3. The peak positions and shapes observed in this work are similar to those prepared using different techniques [17,21,37,39–42]. After lithium insertion (Fig. 6d), the MoO_3 doublet pattern appears as a broadened peak whose deconvolution shows four components, indicating the existence of mixed oxidation states. The peaks at 235.8 and 232.7 eV initially assigned to 3d doublet of Mo^{6+} ions in the as-deposited MoO_3 film slightly shifted towards higher energies (235.9 and 232.9 eV) followed by the appearance of a new pair of peaks located at 234.8 and 231.8 eV. These latter values lie between the energies of Mo^{6+} and Mo^{4+} and are assigned to the energies of $3d_{3/2}$ and $3d_{5/2}$ core levels, respectively for Mo^{5+} [21]. This doublet is responsible of the blue coloration of the films as a response to Li^+ intercalation.

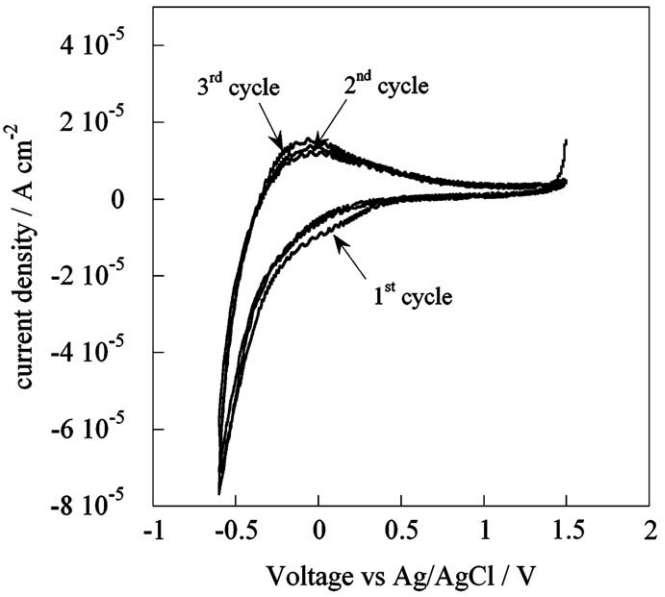

Fig. 7. Cyclic voltammograms (of the as-deposited on ITO glass substrate) after 36 h measured at a sweep rate of 1 mV/s. [Mo^{6+}]: 0.2 mol dm^{-3}, [H_3BO_3]: 0.3 mol dm^{-3}.

There is still some controversy regarding the explanation of the change in the Mo valence state. [43–46] For instance, Faughnan et al. [43] proposed an intervalence in the +6 and +5 oxidation states as the reason for the broad band at 900 nm observed in their absorption spectra, responsible for the blue coloration. Feisch and Mains [44] have reached the same conclusion in their XPS study of UV irradiation and photochromism of MoO_3 and they assumed that the +5 oxidation state of Mo arose from electron transfer from oxygen to molybdenum. However, it is certain that considerable differences in deposition methods and conditions produce differences in structural, optical, morphological, as well as electrochemical properties.

3.4. Electrochemical analysis

Cyclic voltammograms of the deposited h-$MoO_3.nH_2O$ films recorded in the potential range between −0.3 and +1.2 V versus. Ag/AgCl are shown in Fig. 7. MoO_3 film is known to exhibit

electrochromic properties, i.e. change of color in response to an electrically induced change in oxidation state [47]. The phenomenon of electrochromism was observed by the application of external potential between the working electrode and the electrolyte. The photographs of the MoO_3 films before and after the electrochemical tests (see supporting information) are explicit in terms of coloration and bleaching. The as-deposited film was light gray in hue. The reduction peak was associated with a deep coloration of the film while the bleaching process was marked by the oxidation peak. It is well known that the reduction process involves the injection of electron and cationic species into MoO_3 to form molybdenum bronze [17,47,48]. Since the test was conducted in 1 M $LiClO_4$-PC electrolyte solution, we assumed that such a coloration/bleaching process was governed by the double insertion/extraction of electrons and Li^+ ions. The shape of these voltammograms resembles that of Li-doped MoO_3 film fabricated by other techniques [18,37,49]. On the basis of available reports on XPS spectroscopic characterization of MoO_3 films, it has been shown that the electrochromism mechanism of MoO_3 films depends on the existence of different final states such as Mo^{6+} and Mo^{5+} [17,50,51]. Therefore, we conclude that the LPD-based MoO_3 films have demonstrated an electrochromic behavior, even if they displayed low reversibility during electrochemical analysis. Detailed investigations on other properties of this material are in progress and will be presented subsequently.

4. Conclusion

Highly crystallized hexagonal phase $MoO_3.nH_2O$(n∼0.56) films have been successfully fabricated by the liquid phase deposition technique. Despite the low-temperature reaction and without calcination, the intensity and sharpness of XRD peaks indicated that the as-deposited films are highly crystallized. SEM images showed that the deposited nuclei are made of regularly well-shaped hexagonal rods. The amount of deposition and the size of nuclei could be controlled by reaction time. The Gaussian shape of the doublet of Mo 3*d* core level spectrum showed the presence of Mo^{6+} oxidation state in the deposited films. Upon dehydration, the hexagonal $MoO_3.nH_2O$ was transformed into the thermodynamically stable orthorhombic phase at ca. 430 °C. Although not studied in detailed, the obtained films exhibited an electrochromic behavior by lithium intercalation and deintercalation, which resulted in coloration and bleaching. Thus, the LPD method could be regarded as a reliable technique of preparation of well-shaped hexagonal molybdenum trioxide hydrate films with promising technological applications.

Acknowledgments

This study was partly supported by Grant-in-Aid for Scientific Research (a) (Nos. 15205026 and 19205029) and Grant-in-Aid for Scientific Research on Priority Areas (No. 16080211).

Appendix A. Supporting Information

Supplementary data associated with this article can be found in the online version at doi:10.1016/j.jssc.2009.06.033.

References

[1] J.M. Titaboutet, J.E. Germain, C.R. Acad. Sci. Paris, Serie C, 290 (1980) 321.
[2] R.J. Mortiner, Chem. Soc. Rev. 26 (1997) 147.
[3] N.J. Yao, K. Hashimoto, A. Fujishima, Nature 355 (1992) 624.
[4] C.G. Granqvist, A. Azens, A. Hjelm, L. Kullman, G.A. Niklasson, D. Rönnow, M. StrØmme Mattsson, M. Veszelei, G. Vairars, Sol. Energy 63 (1998) 199.
[5] C. Julien, G.A. Nazri, Solid State Ionics 68 (1994) 111.
[6] G. Andersson, A. Magneli, Acta Chem. Scand. 4 (1950) 793.
[7] E.M. McCarron III, J. Chem. Soc. Commun. 336 (1986) 336.
[8] I.P. Olenkova, D.V. Tarasova, G.N. Kustova, G.I. Aleshina, E.L. Mikkailenko, React. Kinet. Catal. Lett. 9 (1978) 221.
[9] M. Figlarz, Prog. Solid State Chem. 19 (1989) 1.
[10] J. Guo, P. Zavalij, M.S. Whittingham, J. Solid State Chem. 117 (1995) 323.
[11] N. Sotani, Bull. Chem. Soc. Japan 48 (1975) 1820.
[12] Y. Iriyama, T. Abe, M. Inaba, Z. Ogumi, Solid state Ionics 135 (2000) 95.
[13] C.V. Ramana, C.M. Julien, Chem. Phys. Lett. 428 (2006) 114.
[14] F.F. Ferriera, T.G. Souza Cruz, M.C.A. Fantini, M.H. Tabacniks, C. de Castro Sandra, J. Morais, A. de Siervo, R. Landers, A. Gorenstein, Solid State Ionics 136–137 (2000) 357.
[15] R. Cárdenas, J. Torres, J.E. Alfonso, Thin Solid Films 478 (2005) 146.
[16] A. Abdellaoui, G. Lêvêque, A. Donnadieu, A. Bath, B. Ouchikhi, Thin Solid Films 304 (1997) 39.
[17] A. Guerfi, R.W. Paynter, L.H. Dao, J. Electrochem. Soc. 142 (1995) 3457.
[18] Y. Zhang, S. Kuai, Z. Wang, X. Hu, Appl. Surf. Sci. 165 (2000) 56.
[19] K. Hinokuma, A. Kishimoto, T. Kubo, J. Electrochem. Soc. 141 (1994) 876.
[20] S. Komaba, N. Kumagai, R. Kumagai, N. Kumagai, H. Yashiro, Solid State Ionics 152–153 (2002) 319.
[21] M.A. Bica de Moraes, B.C. Trasferetti, F.P. Rouxinol, R. Landers, S.F. Durrant, J. Scarmínio, A. Urbano, Chem. Mater. 16 (2004) 513.
[22] A. Hishinuma, T. Goda, M. Kitaoka, S. Hayashi, H. Kawahara, Appl. Surf. Sci. 48/49 (1991) 405.
[23] S. Deki, Hnin Yu Yu Ko, T. Fujita, K. Akamatsu, M. Mizuhata, A. Kajinami, Eur. Phys. J. D 16 (2001) 325.
[24] S. Deki, S. Iizuka, A. Horier, M. Mizuhata, A. Kajinami, Chem. Mater. 16 (2004) 1747.
[25] H. Nagayama, H. Honda, H. Kawahara, J. Electrochem. Soc. 135 (1988) 2015.
[26] H. Parikh, M.R. De Guire, J. Cer. Soc. Japan. 117 (2009) 228.
[27] T.P. Niesen, M.R. De Guire, Solid State Ionics 151 (2002) 61.
[28] S. Deki, A. Hosokawa, A.B. Béléké, M. Mizuhata, Thin Solid Films 517 (2009) 1546.
[29] S. Deki, Y. Aoi, Y. Asaoka, Y. Kajinami, M. Mizuhata, J. Mater. Chem. 7 (1997) 733.
[30] J. Song, X. Ni, L. Gao, H. Zheng, Mater. Chem. Phys. 102 (2007) 245.
[31] S.R. Dhage, M.S. Hassan, O.B. Yang, Mater. Chem. Phys. 114 (2009) 511.
[32] V.V. Atuchin, T.A. Gavrilova, V.G. Kostrovsky, L.D. Pokrovsky, I.B. Troitskaia, Inorg. Mater. 44 (2008) 622.
[33] C.V. Ramana, V.V. Atuchin, I.B. Troitskaia, S.A. Gromilov, V.G. Kostrovsky, G.P. Saupe, Solid State Commun. 149 (2009) 6.
[34] J. Song, X. Wang, X. Ni, H. Zheng, Z. Zhang, M. Ji, T. Shen, X. Wang, Mater. Res. Bull. 40 (2005) 1751.
[35] S. Deki, N. Yoshida, Y. Hiroe, K. Akamatsu, M. Mizuhata, A. Kajinami, Solid State. Ionics 151 (2002) 1.
[36] X.W. Lou, H.C. Zeng, Chem. Mater. 14 (2002) 4781.
[37] M. Kharrazi, A. Azens, A. Hjelm, L. Kullman, C.G. Granqvist, Thin Solid Films 295 (1997) 117.
[38] N. Ikeo, Y. Iijima, N. Niimura, M. Sigematsu, M. Tazawa, S. Matsumoto, K. Kojima,Y. Nagasawa, (Ed.), Handbook of X-ray Photoelectron Microscopy, JEOL, March 1991, p. 96.
[39] Z. Li, L. Gao, S. Zheng, Mater. Lett. 57 (2003) 4605.
[40] W. Li, F. Cheng, Z. Tao, J. Chen, J. Phys. Chem. B. 110 (2006) 119.
[41] M. Epifani, P. Imperatori, L. Mirenghi, M. Schioppa, P. Siciliano, Chem. Mater. 16 (2004) 5495.
[42] M. Anwar, C.A. Hogarth, R. Bulpett, J. Mater. Sci. 24 (1989) 3087.
[43] B.W. Faughan, R.S. Crandall, P.M. Heyman, RCA Rev. 36 (1975) 76.
[44] T.H. Fleisch, G.L. Mains, J. Chem. Phys. 76 (1982) 780.
[45] C. Bechinger, S. Ferrere, A. Zaban, J. Sprague, B.A. Gregg, Nature 383 (1996) 608.
[46] C. Julien, A. Khelfa, O.M. Hussain, G.A. Nazri, J. Crystal Growth 156 (1995) 513.
[47] R. Sivakumar, C.S. Gopinath, M. Jayachandran, C. Sanjeeviraja, Current Appl. Phys. 7 (2007) 76.
[48] D. Belanger, G. Laperriere, Chem. Mater. 2 (1990) 484.
[49] T. Ivanova, K. Gesheva, F. Hamelmann, G. Popkirov, M. Abrashevc, M. Gancheva, E. Tzvetkovaa, Vacuum 76 (2004) 195.
[50] G. Laperriere, M.A. Lavoie, D. Belanger, J. Electrochem. Soc. 143 (1996) 3109.
[51] K. Gesheva, A. Szekeres, T. Ivanova, Sol. Energy Mater. Sol. Cells 76 (2003) 563.